High-resolution CFD modelling of Lillgrund Wind farm

Creech, Angus C.W.; Fruh, Wolf-Gerrit; Maguire, A Eoghan

Publication date:
2013

Citation for published version (APA):
Creech, A. C. W., Fruh, W-G., & Maguire, A. E. (2013). High-resolution CFD modelling of Lillgrund Wind farm. Paper presented at International Conference on Renewable Energies and Power Quality, Bilbao, Spain.

International Conference on Renewable Energies and Power Quality (ICREPQ'13)
Bilbao (Spain), 20th to 22th March, 2013
Renewable Energy and Power Quality Journal (RE&PQJ)
ISSN 2172-038 X, No.11, March 2013

High-resolution CFD modelling of Lillgrund Wind farm

A.C.W. Creech[1], W.-G. Früh[2] and A.E. Maguire[3]

[1] Institute of Energy Systems, School of Engineering, University of Edinburgh
Kings Buildings, Edinburgh EH9 3JL (UK)
E-mail: a.creech@ed.ac.uk

[2] Institute of Mechanical, Process and Energy Engineering, School of Physical Sciences and Engineering,
Heriot-Watt University, Riccarton, Edinburgh EH14 4AS (UK)
E-mail: w.g.fruh@hw.ac.uk

[3] Vattenfall United Kingdom, Research & Development New Renewables
The Tun, Holyrood Road, Edinburgh EH8 8AE (UK)
E-mail: eoghan.maguire@vattenfall.com

Abstract. We report on a fully dynamic simulation of Vattenfall's Lillgrund offshore Wind Farm, with a focus on the wake effects of turbines on the performance of individual turbines, and of the farm as a whole.

The model uses a dynamic representation of a wind turbine to simulate interaction between the wind and the turbine rotors, calculating the instantaneous power output and forces on the air; this was embedded in a finite element, large eddy simulation (LES) computational fluid dynamics code. This model was applied to the wind farm for a selection of key wind speeds and directions, to investigate cases where a row of turbines would be fully aligned with the wind or at specific angles to the wind. The simulation results were then compared to actual performance measurements from the wind farm spanning several years' of operation.

These results demonstrate that time-resolving LES simulations are able to reproduce realistic wake structures, including wake meandering and wake recovery, as well as the effect of wakes on turbine performance.

Key words
Wind farm modelling, wake effect, CFD, large eddy simulation, wind farm performance.

1. Introduction

Due to the rapid increase in the development of substantial offshore wind farms, estimating the wind farm electricity production reliably has become ever more important. A key factor affecting the performance is that turbines in the array may be in the wakes of upstream turbines where they experience substantially lower wind speeds than the upstream turbines [1]. Common approaches are Reynolds-Averaged Navier-Stokes (RANS) CFD or simpler flow modelling coupled with linear wake theory, such as Jensen's Park model. However, it is recognised that the simple wake models lose accuracy when applied to multiple wakes interacting.

Recent research has combined simple turbine models with flow models, with turbines often represented as simple porous discs [2], actuator discs [3], actuator lines [4], or lifting line representations [5]. These can be embedded in RANS fluids solvers [6] or fixed-mesh LES codes [4][7] or an LES finite element solver with an unstructured, hr-adaptive mesh [8].

This paper presents a CFD study using an hr-adaptive LES solver which resolves the wakes fully without the need of analytical wake models. To allow fluid flow at both, turbine and farm scale to be resolved, the turbines are represented as cylindrical volumes, in which rotor lift and drag forces are based upon blade element momentum theory. These are expressed as reaction forces on the fluid which are radially resolved over the rotor area but distributed uniformly in azimuth and distributed axially to provide a realistic yet computationally stable force on the fluid [3]. Furthermore, the consequent torque on the blades accelerates the blades, and provides torque to a virtual generator, to produce continually varying rotor RPM and power outputs. This more realistic approach sets it apart from more common *a posteriori* methods,

Table 1. Table of cases simulated.

Wind direction (deg)	Relative direction (deg)	Case description
198	– 25	2nd row turbines in gap between two front turbines and 3rd row behind 1st row
202	– 21	
207	– 16	
212	– 11	
217	– 6	
223	0	Turbines fully aligned with wind direction
229	6	
236	13	2nd row turbines in gap between two front turbines and 3rd row behind 1st row

where the turbine rotor RPM is either predetermined [9] or calculated directly from the freestream wind speed [10].

The model used here has already been validated against wake measurements of a single turbine [3], and this work represents the extension and application of that model to the fully operational Lillgrund wind farm, situated in the sea between Denmark and Sweden [11], consisting of forty-eight 2.3 MW Siemens turbines.

2. Model configuration

The Computational Fluid dynamics (CFD) solver used in these simulations was the hr-adaptive finite-element solver *Fluidity* [12]. This open-source CFD packages uses the finite-element approach on an unstructured mesh. Among the available turbulence approaches, we adopted large eddy simulation (LES) using a standard Smagorinsky subgrid model. To resolve all 48 turbine wakes with the required resolution for direct modelling of their evolution and recovery, the model had to be run on a parallel computing facility, partly the cluster in the Institute of Petroleum Engineering of Heriot-Watt University and partly at the Edinburgh Parallel Computing Centre.

The three-dimensional computational domain had a square area of 8.1 km by 8.1 km, and a height of 600 m. The wind farm was positioned such that the first turbine was 2 km from the inlet, allowing turbulence to develop fully before encountering the wind farm. The orientation of the domain was kept constant, but the turbines were rotated to account for different wind directions. To provide an adequate resolution at the wind farm and in the wake without using up unnecessary computing resources, an adaptive mesh was used. Far away from the turbines the resolution was 75 m in the horizontal and at least 25 m in the vertical, whilst nearer the turbines, the resolution was a maximum of 5 m both horizontally and vertically. Fluidity's hr-adaptive meshing algorithms would increase the mesh resolution to track flow features such as eddies, and so the finite-element mesh did not remain constant over time.

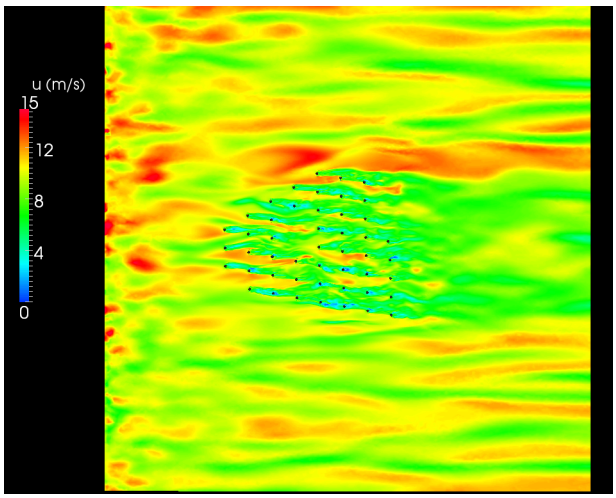

Figure 1. Snapshot of streamwise velocity in a horizontal section at hub height. The grey dots indicate the turbine locations.

The turbines themselves were incorporated into the CFD domain through the definition of cylindrical 'turbine volumes' with the cylinder axis aligned with the turbine's rotor-generator shaft, the same diameter as the rotor diameter and a length of 15 m (~ 0.15*D*). The interaction between the fluid and the turbine is achieved with the model described by Creech et al. [3] through the lift and drag coefficients from the turbine blades distributed uniformly in the azimuthal direction and with a Gaussian weighting in the streamwise direction over the turbine volume. Additionally, some turbulence was generated, especially in the tip region. The lift and drag coefficients were chosen from NACA airfoil data, derived from the specified NACA type [13] for the Siemens turbines installed in Lillgrund.

The turbulent inflow boundary conditions were generated using the Synthetic Eddy Method [14], which produced a logarithmic velocity profile superimposed with fluctuations based upon a Kaimal spectrum (DS 472, 1992) representing the turbulence characteristics of the atmosphere; the mean wind speed at hub height was specified as 10 m/s. The surface roughness of the lower boundary, representing the sea surface was chosen as 2×10^{-4} m, consistent with that shear. After an initial spin-up of the model without active turbines present lasting 2000 s, the turbines were activated and allowed to reach stable operating conditions, as monitored by the power output from the turbines. Typically, the turbine models had reached that level after around 400 to 600 s of model time. The model was then continued for another 600 s, from which the results were taken.

3. Results

We will first present typical flow fields obtained in the simulations, and then compare the power output from the simulations with comparable observations from the SCADA data of the wind farm.

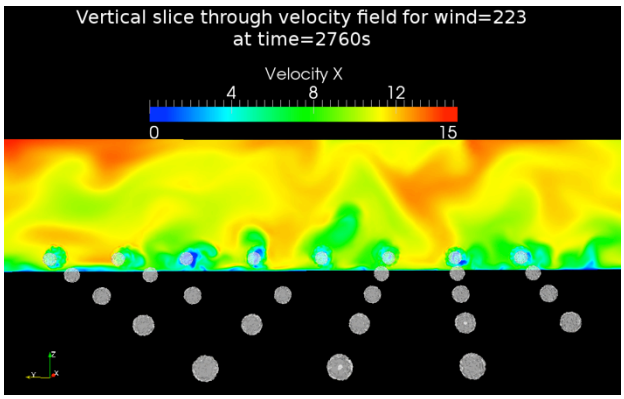

Figure 2. Snapshot of streamwise velocity in a vertical section; close-up in wind farm.

A. Velocity Fields

Figure 1 shows a typical instantaneous velocity field, where the colour scale shows the streamwise velocity, *u*. One can see in Figure 1 that some of the higher frequency turbulence generated at the inlet quickly decays, but at longer length scales persists much further. The individual wakes behind each turbine are clearly visible including substantial wake meandering, as well as some areas where the air is accelerated around the wind farm, and into corridors within the wind farm where jetting is clearly visible. The vertical cross-section in Figure 2 demonstrates the three-dimensional nature of the turbulence, and one can see that the turbines also have an effect on the wind at levels above the turbines. Following the terminology defined by [11], the bottom row of turbines in Figure 1 is referred to as column A, with turbine A07 on the left and turbine A01 on the right end of that column. For the particular wind directions investigated here, turbines B08, C08, and D08 form the front row of turbines, and of particular interest for deep wake effects are columns B, C, and D.

Another noteworthy feature of the flow field in Figure 1 is the large wake behind the entire wind farm which persists as far as the outlet of the computational domain – an *en masse* effect from our individually modelled turbines. Figure 3 shows three cross-sections of the streamwise velocity across the wind farm, with the solid black lines upstream of the wind farm, the dashed red line between the second and third row, and the blue solid line behind the wind farm. The fluctuations in the solid black line represent the free-stream turbulence. The red line clearly shows the individual wakes behind the nearest turbines with a lowest wind speed of around 50% of the freestream velocity. Some distance behind the wind farm (ten rotor diameter behind the last row) the individual wakes have largely merged and now form a wind farm wake with a wake velocity of around 70% of the freestream velocity.

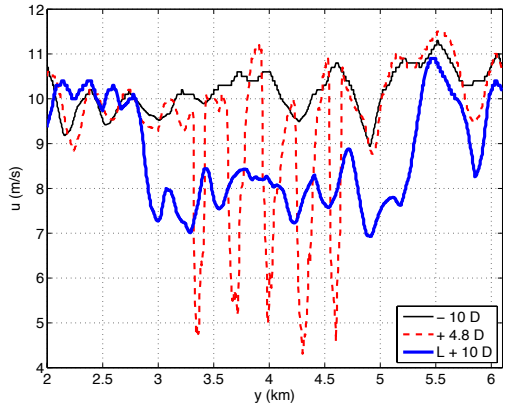

Figure 3. Cross section of the stream wise velocity at hub height, upstream of the wind farm (black solid line), between the second and third row (red dashed line), and downstream of the wind farm (blue solid line).

B. Power deficit

The power output from a column of turbines through the centre of the wind farm (column C, third column from the bottom in Figure 1) is shown in Figure 4. One can clearly see power fluctuations which are consistent with the freestream turbulence. Some of the flow features can be traced through subsequent turbines with a time delay consistent with the wind speed and turbine separation; for example the gust visible in the front (black) turbine at the beginning, then 100 s later in the second turbine (red), and again around 80 s later in the third turbine (green).

To quantify the performance of a turbine unaffected by other turbines, the relative power deficit for each turbine was calculated as the ratio of that turbine's active power divided by a reference power output, where the reference

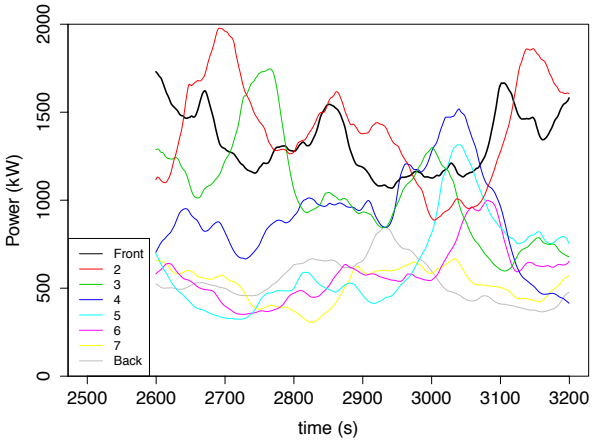

Figure 4. Power output from turbines in column C during final 600 s of computer simulation for the wind direction of 207°.

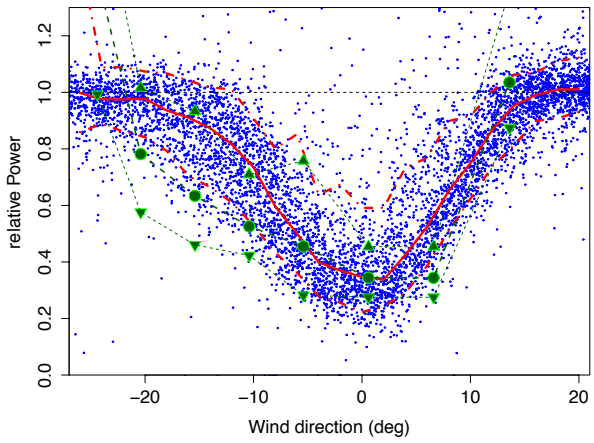

Figure 5. Relative power deficit of turbine D07 in second row compared to front turbine D08. Blue dots: SCADA data; red line: median over 2° window, red dashed lines: range covering 75% of measurements; green circles: median of CFD results, green triangles: range covering 75% of results. Direction 0° denotes turbine row fully aligned with wind.

power output was taken as the median of the power output at that time step from the turbines in the front row, turbines B08, C08, and D08 in this study. As was observed by [11], this ratio is a reliable indicator as long as the turbines operate sufficiently above the cut-in and below the rated conditions.

The average power deficit for a turbine in the second row for the different wind directions is superimposed on the measured power deficit from the wind farm observations in Figure 5 In the observational data, the maximum power deficit was found for a wind direction of around 231°, presumably due to a calibration offset of the instruments on the Met. mast, also noted in [11]. To remove this systematic bias, the wind direction for the observations and the simulations are in the following relative to the observed minimum of 231° and the computational choice of 223°. In this superposition in Figure 5, a clear reduction of the power output from 100% of the front turbine to around 30% can be seen in the observational data represented as the small blue dots. From these data, the median and 75%-range over a 2° window are shown as the red lines. The large green circles and triangles are the median and 75% range, respectively, from the CFD simulations. It is clear that the highly dynamic LES simulations show a substantial variability in the power output which is of the same magnitude as the variability across the Lillgrund data set sampled at 10 minute intervals.

To build up a picture how this wake effect continues deep into the wind farm, the median of the time series of relative power for turbines in column C from all model simulations are shown in Figure 6, where each block of columns refers to a particular turbine, with C08 in the front and C01 at the back. The columns within each block refer to the different wind conditions with the left column corresponding to a wind direction of 198° or –25° relative to the fully aligned case. The right-most column in each block correspondingly refers to the wind direction of 236° or +13°. In steady flow conditions and typical RANS simulations, all columns for the front turbine would be equal to one but since LES captures a substantial amount of instantaneous variability from turbulent eddies, the power output from turbine C08 may vary substantially from the median of the power output of the three front turbines. As a result, the first block of columns shows a noticeable variation from around 90% to around 120%. Compared to the front turbine, the second turbine in Figure 6 shows besides that variability also a systematic change with wind direction, where the second turbine behaves similar to the front turbine at wind directions of 198°, 208°, and 236°. For the other wind directions, the power output of this second turbine is clearly reduced with the most pronounced power deficit at –6° to +6°. Further into the wind farm, the relative power generally decreases to between 40% and 60% of the reference power, and most of the differences across the wind directions are reduced. Some of the turbines, however, appear to show a higher power output than those closer to the front. This could be due to gusts moving through the wind farm, or developing jets as is

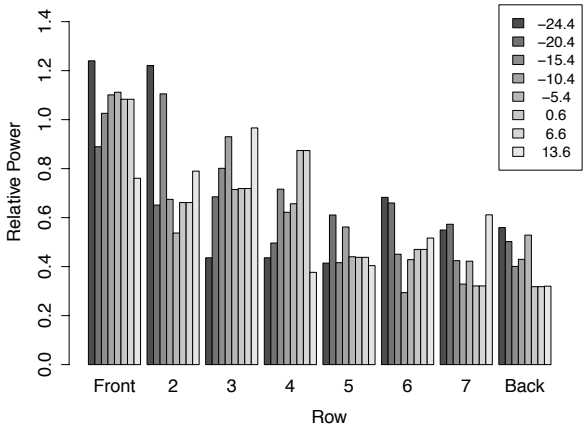

Figure 6. Mean relative power from CFD simulations for column C for the different wind directions as given in legend.

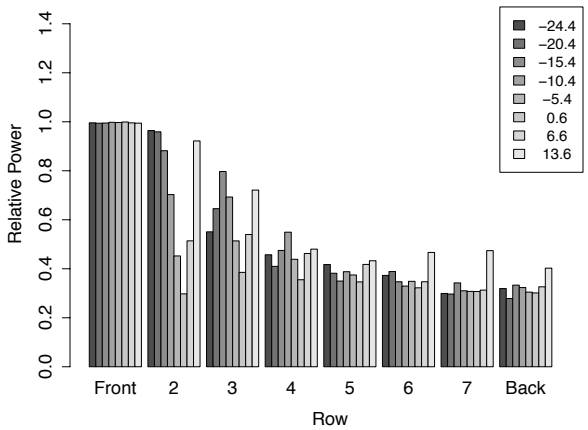

Figure 7. Mean relative power from the observations for column C for the different wind directions as given in legend.

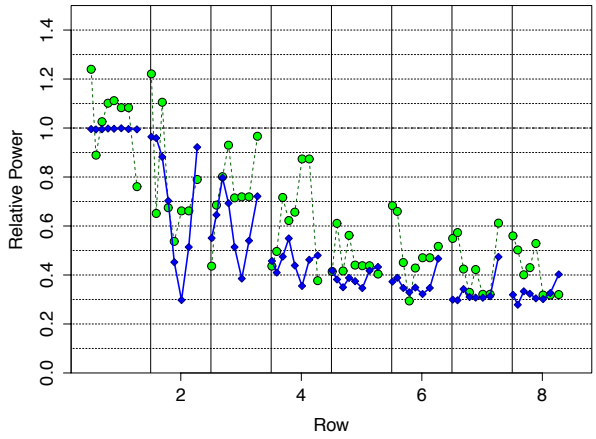

Figure 8. Comparison of mean relative power deficits between CFD simulations (green circles) and observations (blue diamonds) for column C.

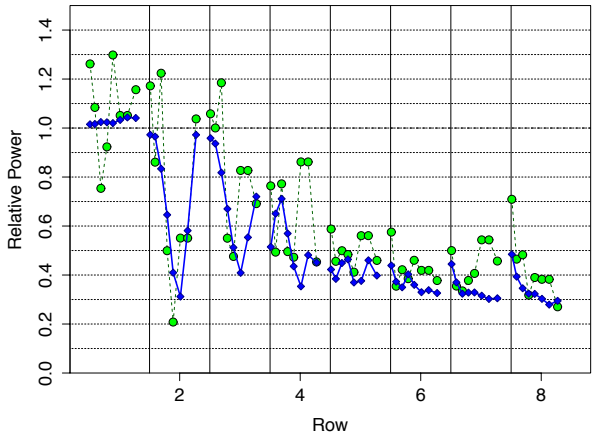

Figure 9. Comparison of mean relative power deficits between CFD simulations (green circles) and observations (blue diamonds) for column B.

possibly seen in Figure 1, where a jet of high velocity air is approaching turbine D02 in the centre of the second line of turbines from the right. The corresponding results from the SCADA data are shown in Figure 7 following the same procedure. Here, the variation across the wind directions for the front turbines are very small, presumably because the wind speed data are 10-minute data and therefore the reference power from the front row of turbines is smoothed out over individual gusts. The second and third turbine show a very strong variation of the power deficit across the wind directions but from the fourth turbine on, the wind direction affects the turbines' output less, with a typical relative output of around 40% of that of the front row turbines.

Figure 8 and Figure 9 show a direct comparison of the computational results with the SCADA data for columns C and B, respectively, by superimposing the computational results as the green circles and the SCADA results as the blue diamonds. Despite the difference across the computational results of a 10-minutes section sampled at a 0.5 second interval and the 10-minute SCADA measurements extracted from a measurement period of over two years, the superposition of these results shows a very consistent picture of a strong directional variation for the turbines in second and third row, where the output is only strongly reduced when the turbines are in line of the wind direction. Deeper into the wind farm, the output is more uniformly reduced to a level for most of the wind directions studied here.

4. Discussion and Conclusions

The high-resolution LES computational model of the Lillgrund wind farm coupled with dynamic modelling of the turbine's interaction with the wind and the resulting power output has successfully reproduced the main observed features gathered from SCADA data of that wind farm over a period of over two years. Unlike Churchfield [4] who reported on highly averaged results, this analysis presents both, the variability found in the unsteady LES simulation as well as that found in the observations from the SCADA data.

In particular, the computations were able to reproduce the power deficit of individual turbines even deep within the wind farm with an accuracy of the same magnitude as given by the spread of the actual observations. This suggests that such models may also be able to successfully model the creation and subsequent decay of the entire wind farm wake.

Features which the computational model showed but are usually not reproduced with RANS, and even unsteady RANS (URANS) CFD models, is the high variability of the flow, originating from the free-stream turbulence initiated at the inlet but also arising from the interaction of the turbines with the flow [6][15]. This leads to substantial wake meandering which, at least phenomenologically, looks similar to that expected for wind farms and also reported by other LES models of wind farms [16] [17]. Moreover, as flow transients larger than the grid resolution are explicit under LES and given that the modelled turbines dynamically react to the flow in a realistic way, their diagnostics also exhibit transience: these may be of value in themselves, especially for reliability analysis of, for example of turbine components subject to fluctuating forces.

Finally, demands on computing power should be mentioned. Despite having a domain 2.5 times larger than the Churchfield Lillgrund model, each simulation using the model described here ran on 256 processing cores, and used 15,000 processor hours; this contrasts with 4096 cores and 1,000,000 processor hours per simulation for Churchfield [4]. There are perhaps several reasons for this. Firstly, Fluidity permits highly anisotropic and variable finite-element meshes to be used in simulation, which through hr-adaptive techniques efficiently

concentrates computing resource in areas of complex flow. Secondly, Churchfield deploys an actuator line technique, which requires much smaller time-steps than actuator discs due the rotating actuator lines within the flow. And yet, despite actuator discs being a more crude representation of turbines than actuator lines, we have demonstrated here that they produce results in good agreement with actual data from Lillgrund. We believe this shows that, with careful choice of CFD and turbine modelling techniques, high-fidelity LES simulations of wind farms on a large scale are a practical and effective resource assessment tool.

Acknowledgement

We would like to acknowledge the support of Vattenfall AB in funding this research. We also thank Ian Chisholm of the Institute of Petroleum Engineering, Heriot-Watt University, and Adrian Jackson of the Edinburgh Parallel Computing Centre, for providing invaluable technical support.

References

[1] R.J. Barthelmie, S.C. Pryor, S.T. Frandsen, K.S. Hansen, J.G. Schepers, K. Rados,WSchlez, A. Neubert, L.E. Jensen, and S. Neckelmann. Quantifying the impact of wind turbine wakes on power output at offshore wind farms. *J. Atmos Ocean Tech*., 27(8):1302 – 1317, 2010.

[2] G. España, S. Aubrun, S. Loyer and P. Devinant. Spatial study of the wake meandering using modeled wind turbines in a wind tunnel. *Wind Energy*, 14:923 – 937, 2011.

[3] A.C.W. Creech. *A three-dimensional numerical model of a horizontal axis, energy extracting turbine*. PhD thesis, Heriot-Watt University, 2009. (Available from: www.ros.hw.ac.uk)

[4] M.J. Churchfield, S. Lee, P.J. Moriarty, L.A. Martínez, S. Leonardi, G. Vijayakumar and J.G. Brasseur. A Large-Eddy Simulation of Wind-Plant Aerodynamics. *50th AIAA Aerospace Sciences Meeting including the New Horizons Forum and Aerospace Exposition*, 2012

[5] E. Machefaux, N. Troldborg, G.C. Larsen, J. Mann and H.A. Madsen. Experimental and numerical study of wake to wake interaction in wind farms. European Wind Energy Association (EWEA) conference, Copenhagen, April 2012, paper 927.

[6] D. Cabezon, E. Migoya, and A. Crespo. Comparison of turbulence models for the computational fluid dynamics simulation of wind turbine wakes in the atmospheric boundary layer. *Wind Energy*, 14(7):909–921, 2011.

[7] Y.-T. Wu and F. Porte-Agel. Large-eddy simulation of wind-turbine wakes: Evaluation of turbine parameterisations. *Boundary-Layer Meteorology*, 138(3):345–366, 2011

[8] A.C.W. Creech, W.-G. Früh and P. Clive. Actuator Volumes and *hr*-adaptive methods for three-dimensional simulation of wind turbine wakes and performance. *Wind Energy*, 15:847 – 863, 2012.

[9] J.N. Sørensen and W.Z. Shen. Numerical modelling of wind turbine wakes. *Journal of Fluids Engineering*, 124:393–399, 2002.

[10] Niels Troldborg, Gunner C. Larsen, Helge A. Madsen, Kurt S. Hansen, Jens N. Sorensen, and Robert Mikkelsen. Numerical simulations of wake interaction between two wind turbines at various inflow conditions. *Wind Energy*, 14(7):859–876, 2011

[11] Jan-Åke Dahlberg. Assessment of the Lillgrund Windfarm: Power Performance, Wake Effects. *Technical report*. Vattenfall AB, September 2009.

[12] M.D. Piggott et al. h, r, and hr adaptivity with applications in numerical ocean modelling. *Ocean Modelling*, 10:95–113, 2004.

[13] APPENDIX 1 - Technical Specification of the Siemens 2.3-MW Mk II Wind Turbine. LWECS Site Permit Application. 2006

[14] N. Jarrin et al. A synthetic eddy method for generating inflow conditions for large-eddy simulations. *Int. J. Heat and Fluid Flow*, 27:585–593, 2006.

[15] R. J. Barthelmie, K. Hansen, S. T. Frandsen, O. Rathmann, J. G. Schepers, W. Schlez, J. Phillips, K. Rados, A. Zervos, E. S. Politis, and P. K. Chaviaropoulos. Modelling and measuring flow and wind turbine wakes in large wind farms offshore. *Wind Energy*, 12:431–444, 2009.

[16] M. Calaf, C. Meneveau, and J. Meyers. Large eddy simulation study of fully developed wind-turbine array boundary layers. *Physics of Fluids*, 22:015110, 2010.

[17] G.C. Larsen, Helge Aa Madsen, Kenneth Thomsen, and Torben J. Larsen. Wake meandering: A pragmatic approach. *Wind Energy*, 11(4):377–395, 2008.